Acta Crystallographica Section D
Biological Crystallography
ISSN 0907-4449

The structure of human neuronal Rab6B in the active and inactive form

Isabel Garcia-Saez,‡ Sergey Tcherniuk‡ and Frank Kozielski*

Laboratoire des Moteurs Moléculaires (LMM), Institut de Biologie Structurale (CEA–CNRS–UJF), 41 Rue Jules Horowitz, 38027 Grenoble CEDEX 01, France

‡ These authors contributed equally.

Correspondence e-mail: frank.kozielski@ibs.fr

Received 13 December 2005
Accepted 26 April 2006

PDB References: Rab6B–GDP, 2fe4, r2fe4sf; Rab6B–GTPγS, 2ffq, r2ffqsf.

The Rab small G-protein family plays important roles in eukaryotes as regulators of vesicle traffic. In Rab proteins, the hydrolysis of GTP to GDP is coupled with association with and dissociation from membranes. Conformational changes related to their different nucleotide states determine their effector specificity. The crystal structure of human neuronal Rab6B was solved in its 'inactive' (with bound MgGDP) and 'active' (MgGTPγS-bound) forms to 2.3 and 1.8 Å, respectively. Both crystallized in space group $P2_12_12_1$, with similar unit-cell parameters, allowing the comparison of both structures without packing artifacts. Conformational changes between the inactive GDP and active GTP-like state are observed mainly in the switch I and switch II regions, confirming their role as a molecular switch. Compared with other Rab proteins, additional changes are observed in the Rab6 subfamily-specific RabSF3 region that might contribute to the specificity of Rab6 for its different effector proteins.

1. Introduction

Small GTP-binding proteins, which are ubiquitous in eukaryotes, form a huge superfamily of proteins with a wide range of cellular roles. According to their functions, they can be classified into at least five distinct structural families (Ras, Rho/Rac/Cdc42, Rab, Sar1/Arf and Ran; Takai *et al.*, 2001). From a structural point of view, they all share the same GDP/GTP-binding topology.

Members of the Rab small G-protein family form the largest branch of the superfamily, with about 70 known Rab proteins identified in the human genome (Bock *et al.*, 2001). Rab proteins can be unequivocally identified by specific 'Rab-conserved' sequences, designated 'Rab-family (RabF) motifs', that cluster around two switch regions called switch I and switch II (Pereira-Leal & Seabra, 2000). They play important roles as regulators of vesicle traffic, including budding, targeting, docking/tethering and fusion of vesicles (Zerial & McBride, 2001). A feature of Rab proteins is that hydrolysis of GTP to GDP (the GDP/GTP cycle) is coupled with the association with and dissociation from membranes: the GDP-bound form of Rab protein in complex with its Rab GDP dissociation inhibitor (GDI) is inactive and localized in the cytosol until released and delivered to its specific membrane compartment. Subsequently, the GDP-bound inactive form is converted by the GDP–GTP exchange factor (GEF) into the GTP-bound form, thus becoming activated and able to interact with its downstream effector(s). Subsequently, the GTP-bound form is converted back to the GDP-bound form

by a protein called GTPase-activation protein (GAP), which allows reformation of the Rab–GDI complex. This complex eventually returns to the cytosol, thus closing the cycle. The GDP/GTP cycle of Rab proteins is coupled to conformational changes mainly occurring in the switch I and switch II regions that in the GTP-bound form allow recognition by their effector proteins. Knowledge of the nucleotide-dependent structural changes of Rab proteins is therefore essential to understanding their interaction with effectors.

At least ten different subfamilies have been identified by their Rab subfamily-specific sequence motifs (RabSF; Moore *et al.*, 1995). Members of the Rab6 subfamily are regulators of membrane traffic from the Golgi apparatus towards the endoplasmatic reticulum (ER; Martinez *et al.*, 1994; White *et al.*, 1999) and are in general expressed ubiquitously. Two different Rab6 genes located in chromosomes 11 and 3, named Rab6A (Zahraoui *et al.*, 1989) and Rab6B (Opdam *et al.*, 2000), respectively, share high sequence identity, but have several different functions identified to date. Two Rab6A isoforms, Rab6A and Rab6A′, are expressed ubiquitously and differ only in three residues (Echard *et al.*, 2000; Shan *et al.*, 2000). The two isoforms Rab6A and Rab6A′ are involved sequentially in the control of the retrograde transport between endosomes and endoplasmic reticulum (ER) *via* the Golgi apparatus (White *et al.*, 1999). Rab6A′ has been proposed to be involved in drug resistance in MCF7/adrR cells (Shan *et al.*, 2000) and is implicated in the direct transport of the Shiga toxin between endosomes and the trans-Golgi network (Mallard *et al.*, 2002). In contrast, Rab6B, which also functions in retrograde membrane traffic at the level of the Golgi complex, is tissue- and cell-type specific and is predominantly expressed in the brain (Opdam *et al.*, 2000). Rab6A and Rab6B have distinct biochemical and cellular properties. Rab6B displays lower GTP-binding activity and is mainly distributed over the Golgi and ER membranes, whereas Rab6A is more restricted to the Golgi apparatus (Opdam *et al.*, 2000). At the protein level, Rab6B displays 91% sequence identity when compared with Rab6A, with differences mainly in the hypervariable C-terminal region of the protein.

Activated Rab6A and Rab6B interact with multiple effectors, including the Rab6 GTPase-activating protein GAPCenA, which partially localizes in the centrosomes (Cuif *et al.*, 1999), Rab6IP2A and Rab6IP2B, two proteins, possibly isoforms of the same gene, with no significant homology to other known proteins which are recruited by activated Rab6 on the Golgi membranes (Monier *et al.*, 2002), the adaptor protein mint3 that links Rab6 to the amyloid precursor protein traffic (Teber *et al.*, 2005) and Rabkinesin-6 (Echard *et al.*, 1998), a motor protein of the kinesin superfamily (Lai *et al.*, 2000). Rabkinesin-6 is associated with the Golgi apparatus and is implicated in the movement of tubules in the retrograde transport that connects the Golgi with the ER. Rabkinesin-6 is overexpressed in dividing cells and its depletion blocks cytokinesis. This suggests that Rabkinesin-6 is involved in the mechanisms that connect membrane traffic to mitotic events (Fontijn *et al.*, 2001). Interestingly, Rab6A′ does not interact with Rabkinesin-6 (Echard *et al.*, 2000), suggesting that the modification of only three residues may have an impact on the effector specificity and thus the function of Rab6 GTPase.

Here, we present the crystal structure of human Rab6B in the 'inactive' GDP-bound and 'active' GTP-bound forms (using the non-hydrolysable GTP analogue GTPγS) to 2.3 and 1.8 Å resolution, respectively. Both crystals belong to the space group $P2_12_12_1$ and have similar unit-cell parameters, giving us the possibility of comparing both structures with an almost identical crystal-packing environment.

2. Experimental

2.1. Materials

The cDNA for *Homo sapiens* Rab6B was purchased from Origene Technologies Inc. GTPγS was purchased from Sigma. The Taq PCR Master Mix Kit was from Qiagen. Restriction enzymes were from New England Biolabs and the The Rapid DNA Ligation Kit was obtained from Boehringer. The *Escherichia coli* pET28a vector was obtained from Novagen. Competent TOP10 and BL21(DE3) cells were from Invitrogen and Novagen, respectively. IPTG was from ICN. The HisTrap FF and HiPrep 26/10 desalting columns were purchased from Amersham Biosciences. Amicon Ultra-4 (10 kDa) was obtained from Millipore. Crystallization kits and 24-well VDX plates were obtained from Hampton Research. 96-well crystallization plates were from Greiner BIO1.

2.2. Cloning

The following forward and reverse primers were used to clone $Rab6B_{13–174}$, truncated at both termini, by standard methods into the *E. coli* pET28a His-tag vector: Rab6B_1, 5′-GAT TTT GGG AAT C**CC ATG G**GA AAA TTC AAG TTG-3′, and Rab6B_2, 5′-CTG GAC ATT CTC CAT **CTC GAG** TAG AGC CGA CGC CAC-3′. The PCR product was generated with Taq polymerase using the full-length Rab6B cDNA as a template. After digestion with *Nco*I and *Xho*I, the PCR product was ligated into pET28a and transformed into competent TOP10 cells. Plasmids isolated from colonies that tested positive for the presence of the desired insert were sequenced to confirm the correctness of the cloning strategy. The expression clone codes for the $Rab6B_{13–174}$ fragment and eight additional residues (LEHHHHHH) at the C-terminus of the protein.

2.3. Protein expression and purification

The plasmid of $Rab6B_{13–174}$ was transformed into competent BL21(DE3) cells and grown at 310 K in 1 l bottles until an optical density ($A_{600\,nm}$) of about 1.0 was reached. The cultures were cooled to 293 K, induced with 0.5 m*M* IPTG and grown for an additional 20 h. Cells were harvested by centrifugation, frozen in liquid nitrogen and stored at 193 K. All subsequent steps were performed at 277 K using an FPLC. The cell pellet was resuspended in buffer *A* (20 m*M* PIPES pH 7.6, 100 m*M* NaCl, 5 m*M* $MgCl_2$, 0.2 mg ml^{-1} DNAse, 0.5 mg ml^{-1} lysozyme), lysed twice using a French Press and centrifuged at ∼10 000*g* for 15 min. The soluble fraction was applied onto a

Table 1
X-ray data collection and structure refinement of Rab6B–GDP and Rab6B–GTPγS.

Values in parentheses are for the last resolution shell: 2.42–2.30 Å for Rab6b–GDP and 1.88–1.78 Å for Rab6b–GTPγS.

	Rab6b–GDP†	Rab6b–GTPγS‡
Data-collection statistics		
Resolution limits (Å)	2.3	1.78
Space group	$P2_12_12_1$	$P2_12_12_1$
Unit-cell parameters		
a (Å)	36.04	35.89
b (Å)	61.13	60.98
c (Å)	66.63	63.69
$\alpha = \beta = \gamma$ (°)	90	90
Reflections		
Measured	46733	90595
Unique	6318	13772
Completeness (%)	92 (100)	97.8 (99.4)
Multiplicity	7.3	6.5
R_{sym}§ (%)	0.052 (0.076)	0.048 (0.209)
$I/\sigma(I)$	10.2	11.9
Structure refinement		
No. of reflections	6292	13561
R_{work} (%)	22.19	19.14
R_{free} (%)	25.68	20.24
R.m.s.d. bond length (Å)	0.00835	0.0058
R.m.s.d. angles (°)	1.80	1.34

† Data collection took place on the ID14-2 X-ray beamline at the European Synchrotron Radiation Facility (ESRF), Grenoble, France. ‡ Data collection took place on the BM30A beamline at the ESRF, France. § $R_{sym} = \sum|I_j - \langle I\rangle|/\sum\langle I\rangle$, where I_j is the intensity for reflection j and $\langle I\rangle$ is the mean intensity.

1 ml HisTrap FF column previously equilibrated in buffer *A* and extensively washed with buffer *B* (20 m*M* PIPES pH 7.6, 100 m*M* NaCl, 20 m*M* imidazole) until the OD_{280} dropped to zero. $Rab6B_{13–174}$ was eluted with buffer *C* (20 m*M* PIPES pH 7.6, 100 m*M* NaCl, 500 m*M* imidazole) and the protein-containing fractions pooled. The protein was applied onto a Hi-Prep 26/10 desalting column previously equilibrated in buffer *D* (20 m*M* PIPES pH 7.6, 100 m*M* NaCl, 2 m*M* DTT) to remove imidazole from the protein. Protein-containing fractions were pooled and concentrated by ultrafiltration using an Amicon Ultra-4 (10 kDa) to a concentration between 10 and 12 mg ml^{-1}. The quality and purity of $Rab6B_{13–174}$ were tested by SDS–PAGE, N-terminal protein sequencing and mass spectrometry; the protein solution was subsequently used for crystallization trials avoiding freezing and thawing.

2.4. Protein crystallization

Crystals of Rab6B with bound MgGDP were obtained with commercially available Hampton crystallization screens using a Cartesian nanodrop crystallization robot. Rab6B at 10–12 mg ml^{-1} (without adding any nucleotide) was mixed in a 1:1 ratio with 588 different precipitation conditions using 100 nl protein and 100 nl precipitant in flat-bottomed 96-well crystallization plates using the sitting-drop method. The plates were stored at 282 K. Crystals appeared after 2 d as bundles of long needles under conditions from the PEG/Ion Screen (0.1 *M* sodium acetate pH 5.0, 0.15 *M* ammonium nitrate and 20% polyethylene glycol 3350). Crystals were then reproduced and improved manually by increasing the drop size to 2 µl using 24-well VDX plates. The best crystals were obtained by increasing the PEG 3350 concentration to 23%. Crystals of Rab6B with bound GTPγS were obtained as follows: the stock protein solution of Rab6B–GDP was supplemented with 5 m*M* $MgCl_2$ and 2 m*M* GTPγS and incubated for 1 h at 277 K. Crystals were grown at room temperature by the hanging-drop vapour-diffusion method with 0.2 *M* ammonium nitrate and 20% polyethylene glycol 3350 pH 6.3. Rab6B–GDP crystallized in space group $P2_12_12_1$, with unit-cell parameters a = 36.04, b = 61.13, c = 66.63 Å. The solvent content was calculated to be 33.2% with one molecule per asymmetric unit. Similarly, Rab6B with bound GTPγS crystallized in space group $P2_12_12_1$, with unit-cell parameters a = 35.89, b = 60.98, c = 63.69 Å. The solvent content for this crystal was 29.7% with one molecule per asymmetric unit.

2.5. Data collection

Data sets from Rab6B–GDP and Rab6B–GTPγS crystals were collected at beamlines ID14-2 and BM30A, respectively, at the European Synchrotron Radiation Facility (ESRF), Grenoble, France. Data were processed with the *DENZO*/*SCALEPACK* program suite (Otwinowski & Minor, 1997) as well as with *SCALA* from the *CCP*4 package (Collaborative Computational Project, Number 4, 1994). The Rab6B–GDP and Rab6B–GTPγS data sets contained data to 2.3 and 1.78 Å resolution, with completenesses of 92 and 98%, respectively (Table 1).

2.6. Structure determination and refinement

The Rab6B–GDP structure was solved by molecular replacement using *AMoRe* (Navaza & Saludjian, 1997). The structure of Rab6A′ complexed with GDP from *Plasmodium falciparum* (PDB code 1d5c) without ions, GDP or water molecules was used as a starting model. The correct solution, after performing a one molecule per asymmetric unit search, yielded a correlation coefficient of 28.0% and an R factor of 47.8%. After an initial round of rigid-body refinement, the model was rebuilt manually using *TURBO-FRODO* (Roussel & Cambillau, 1991). A molecule of GDP, one Mg^{2+} ion and several water molecules were included at the initial stages. The model was further refined by cycles of simulated annealing, energy minimization and *B*-factor refinement using *CNS* (Brünger *et al.*, 1998) and subsequent manual model building. After these initial rounds of refinement, R_{free} remained high owing to disorder around the switch I and switch II regions. To improve phases and reduce model bias, we used the phases from molecular replacement to perform density modification (solvent flipping) and to calculate figure-of-merit weighted Fourier synthesis maps with the calculated phases using *CNS*. In parallel, we started the structural determination of Rab6B–GTPγS. This crystal structure was also solved by molecular replacement using *AMoRe* and our partially refined structure of Rab6B–GDP as a model. The correct solution, after performing a one molecule per asymmetric unit search, yielded a correlation coefficient of 48.5% and an R factor of 41.9%. We performed an initial round of rigid-body refine-

ment, density modification using solvent flipping and figure-of-merit weighted Fourier synthesis maps with the calculated phases using *CNS*. The model was rebuilt manually. A molecule of GTPγS, one Mg^{2+} ion and several water molecules located in the nucleotide-binding site were included. This structure was considerably less disordered and consequently easier to build and refine than the GDP-bound form. The fully refined Rab6B–GTPγS (R_{free} = 20.24%) structure was again used as a template for a new round of molecular replacement for Rab6B–GDP using *AMoRe*. This yielded a correlation coefficient of 53.5% and an *R* factor of 38.6%. Further rigid-body refinement, rounds of energy minimization, *B*-factor refinement and density modification by solvent flipping (*CNS*) followed by model building helped us to refine the Rab6–GDP structure (R_{free} = 25.68%). The final refinement statistics are given in Table 1. The quality of the models was accessed with *PROCHECK* (Laskowski *et al.*, 1993).

For structural comparisons, a superposition between structures was calculated using *LSQKAB* and temperature-factor analysis was performed using *BAVERAGE*, both from the *CCP*4 program suite (Collaborative Computational Project, Number 4, 1994).

2.7. Preparation of figures

Figs. 1(*a*), 2, 3(*a*) and 5 were prepared using *PyMOL* (DeLano, 2002). The structural and sequence alignment in Figs. 1(*b*) and 3(*b*) were performed using *ESPript* (Gouet *et al.*, 1999) and modified by hand. In Fig. 4, average *B* factors and main-chain r.m.s.d. data were plotted using *Microsoft Excel* 2004 for Macintosh (v.11.1).

3. Results

Human Rab6B is a protein of 208 residues with a 13-residue N-terminal stretch, a catalytic domain that contains the GTP-binding motifs, including the switch I and switch II regions, and an approximately 30-residue-long C-terminal hypervariable region and a cysteine motif (C*X*C) responsible for prenylation of membranes (Fig. 1*b*). A truncated Rab6B protein was cloned (Lys13–Leu174), expressed and purified to homogeneity and is used for structural studies. Owing to bacterial excision (Hirel *et al.*, 1989), the first methionine is missing, as shown by N-terminal protein sequencing (GKFKLVL). When examined by electrospray mass spectrometry, the measured weight of 19 768 Da was shown to be in good agreement with the theoretical value calculated from the primary sequence (19 765 Da, taking the additional residues LEHHHHHH into account). Rab6B$_{13–174}$ is predominantly monomeric in solution (data not shown). To better understand the nucleotide-dependent conformational changes that lead to recognition of the different effector proteins by Rab6B, we solved the crystal structures of Rab6B in the 'active' (GTPγS-bound, which is believed to interact with Rabkinesin-6) and 'inactive' (GDP-bound) form using molecular replacement with the *P. falciparum* Rab6A′–GDP structure as a starting model. Overall Rab6B adopts the classical fold for Ras-like small GTPases with a six-stranded mixed β-sheet (β1–β6; only β2 is antiparallel) surrounded by five α-helices (α1–α5; Fig. 1*a*). There are no striking differ-

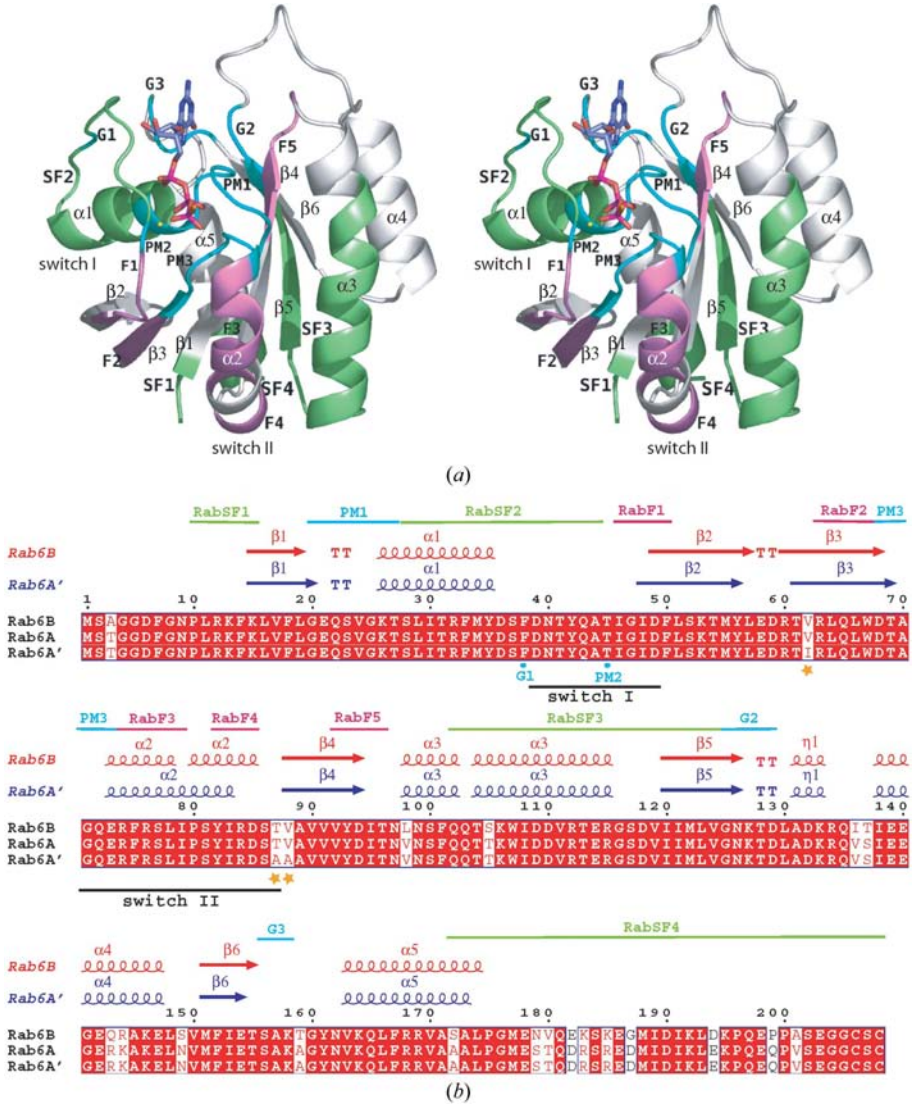

Figure 1
(*a*) Stereoview of the crystal structure of Rab6B–GTPγS. RabF and RabSF regions are depicted in violet (F1–F5) and green (SF1–SF4), respectively. Consensus domains for phosphate/magnesium binding (PM1–PM3) and guanine nucleotide binding (G1–G3) are shown in cyan. (*b*) Structural and sequence alignment of human Rab6B (our structure), RabA′ (PDB code 1yzq) and RabA. Identical residues are in white on a red background; similar residues are in red with a white background. The three residues that differ between RabA and RabA′ are indicated with an orange star.

ences in the secondary-structure elements compared with other Rab proteins.

3.1. The structure of Rab6B in the GTPγS-bound state

The structure of GTPγS-bound Rab6B is well defined, comprising residues Lys13–Leu174 and two additional residues (Leu and Glu) linking the protein to the C-terminal histidine tag (not visible in our structure). The structure includes one magnesium ion, non-hydrolysable GTPγS and 132 water molecules. The overall Mg-GTPγS-bound structure is shown in Fig. 1(*a*). The positions of the switch I and switch II regions, Rab family-specific (F1–F5) and Rab6 subfamily-specific (SF1–SF4) motifs, the guanine-binding motifs (G1, G2 and G3) that interact with the guanyl group and the phosphate/magnesium-binding motifs (PM1, PM2 and PM3) that interact with either magnesium and/or the phosphate groups are indicated. Electron density is reasonably well defined even in the loop regions. Mg-GTPγS is located in an open pocket formed by the six nucleotide-binding motifs and makes a large number of main- and side-chain interactions. The Mg^{2+} is octahedrally coordinated by the hydroxyl groups of Thr45 (PM2) and Thr27 [PM1, also called the P-loop (G*XXXX*GKS/T)], one O atom of the β- and γ-phosphates and two water molecules. Lys26 (PM1) and the main-chain N of Gly71 (PM3) interact with the O1 atom of γ-phosphate, while O2 binds to one water molecule and the main-chain N of Thr45 (PM2). The sulfur from the γ-phosphate interacts with the hydroxyl group of Tyr42 (switch I) and with the main-chain N of Ser23 (PM1). One oxygen of the β-phosphate makes contact with the main-chain N atoms of Val24, Gly25 and Lys26 and the Lys26 side chain, all of which are located in the PM1 motif. The other oxygen binds to one water molecule and the Lys26 and Thr27 main-chain N atoms (PM1). O1 from the α-phosphate interacts with the Ser28 and Thr27 main-chain N atoms (PM1), whereas O2 binds to two water molecules. The ribose maintains contacts with several residues including the main-chain N atom of Tyr42, the side chain of Lys127 and one water molecule. The guanyl group makes an edge-to-edge aromatic interaction with Phe38 (G1), which is approximately perpendicular to the guanyl group, and also makes contacts with the side chain and main chain of Asn126 (G2), the side chain of Asp129 (G2) and the main chain of Ala157 and Lys158 (G3).

3.2. The GDP-bound state

Crystals of Rab6B in the inactive GDP-bound form diffract to 2.3 Å, belong to the same space group and have unit-cell parameters similar to those of GTPγS–Rab6B (Table 1). The structure with GDP in the active site comprises residues Phe14–Leu174, a molecule of GDP, an Mg^{2+} ion, 79 water molecules and a nitrate ion. In the nucleotide-binding site, the contacts between the guanyl and ribosyl grops and the α- as well as the β-phosphate of GDP with the protein are the same as those observed for GTPγS. The nitrate group, probably from the crystallization buffer, occupies the space of the absent γ-phosphate group and establishes interactions with Lys26 (PM1), Thr45 (PM2), Mg^{2+}, the two O atoms of the β-phosphate of GDP and one water molecule. Even though the nitrate ion is located in a position similar to that of the γ-phosphate in the GTPγS complex, it does not interact with any residue of PM3 (included in switch II). This fact and the high flexibility of the region indicate that the presence of the nitrate ion does not simulate the binding of a γ-phosphate group. However, it may help to stabilize the GDP in the active site; as in the GTPγS structure, Mg^{2+} is also octahedrally coordinated, with the position of the missing γ-phosphate O atom now occupied by an oxygen from the nitrate group. However, the interactions with the main chains or side chains of residues located in the PM1–PM3 nucleotide-binding regions maintained by γ-phosphate are no longer present to stabilize the structure, as observed in the GTPγS-bound form (Fig. 2). As a consequence, the switch I and switch II regions shift their positions compared with the GTPγS-bound form (Fig. 3), whereas the rest of the Rab6B structure overall remains unchanged. In the GDP-bound state the electron density for both regions is

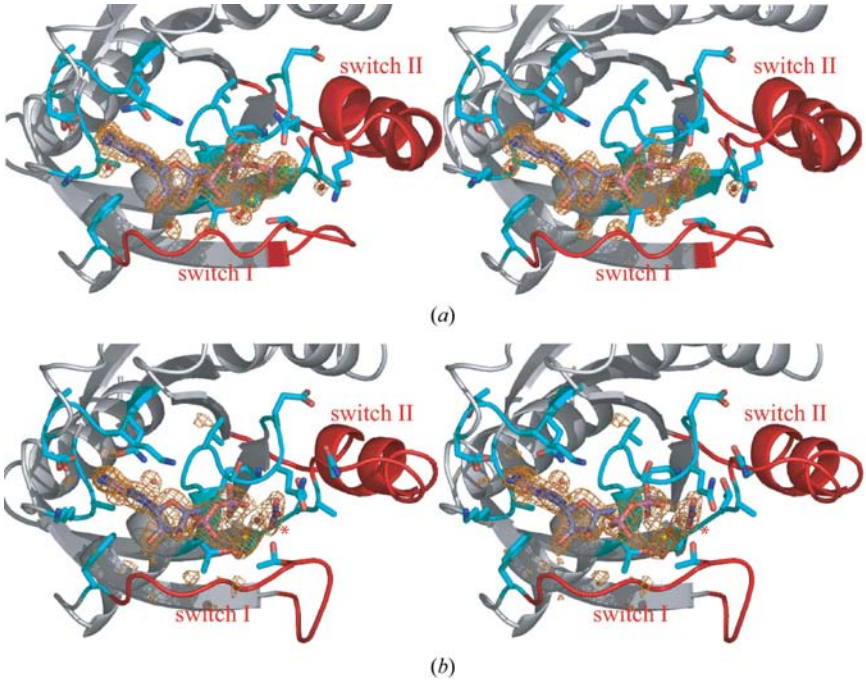

Figure 2
Stereoview of the nucleotide-binding site of (*a*) Rab6B–GTPγS and (*b*) Rab6B–GDP. Switch I and II are depicted in red. The residues for the phosphate/magnesium binding (PM1–PM3) and guanine-nucleotide binding (G1–G3) are shown in cyan. $F_o - F_c$ maps calculated omitting the nucleotides, Mg and water molecules of the nucleotide-binding site area are contoured at 2.5σ. In (*b*), the molecule of nitrate is indicated with an asterisk.

weak and not well defined, confirming the implication of this area in sensing the different nucleotidic states that provoke the switch between 'inactive' (GDP-form) and 'active' (GTP-form) states.

3.3. Comparison between GTPγS- and GDP-bound forms

Both GTPγS- and GDP-bound Rab6B forms crystallized in the same orthorhombic space group, with similar unit-cell parameters and crystal packing. This allows a direct comparison of both nucleotide-bound states (Fig. 3). Structural superposition between Rab6B–GTPγS and Rab6B–GDP gave a main-chain root-mean-square deviation (r.m.s.d.) of 0.8 Å. The high flexibility of the switch regions is reflected by comparing the *B* factor for the GDP-bound and GTPγS-bound forms. Both structures have similar overall *B* values for all atoms (17.6 for the GTPγS-bound form and 23.7 for the GDP-bound state), but the strongest differences are concentrated in the switch areas. Detailed comparisons between the average *B* factors per residue for both structures and main-chain r.m.s.d.s calculated between both GDP and GTPγS forms highlight these differences (Fig. 4). These are located around the switch I, switch II and, interestingly, in the subfamily-specific RabSF3 region, more particularly around the C-terminal section of helix α3 and the following loop which connects to β5. Comparisons of surface representations of both structures reveal conformational changes between the two states in these regions (Fig. 5). The surface in Rab6B GTPγS undergoes conformational changes which lead to a more compact surface, where polar residues such as Glu73 and Arg76 point out from the switch II region and are exposed to the solvent (Figs. 5*a* and 5*b*), as does Arg63, which neighbours Val62, one of the three residues that are different in Rab6A′ (Figs. 5*c* and 5*d*).

The RabSF3 conformations are stabilized by a relatively small number of intermolecular interactions. In the GTPγS-bound form we found seven hydrogen bonds with two symmetry-related molecules which involve Asp109, Thr113 and Ser117. In the GDP-form we found only three intermolecular hydrogen bonds and these involve Asp109, Arg112 and Thr113.

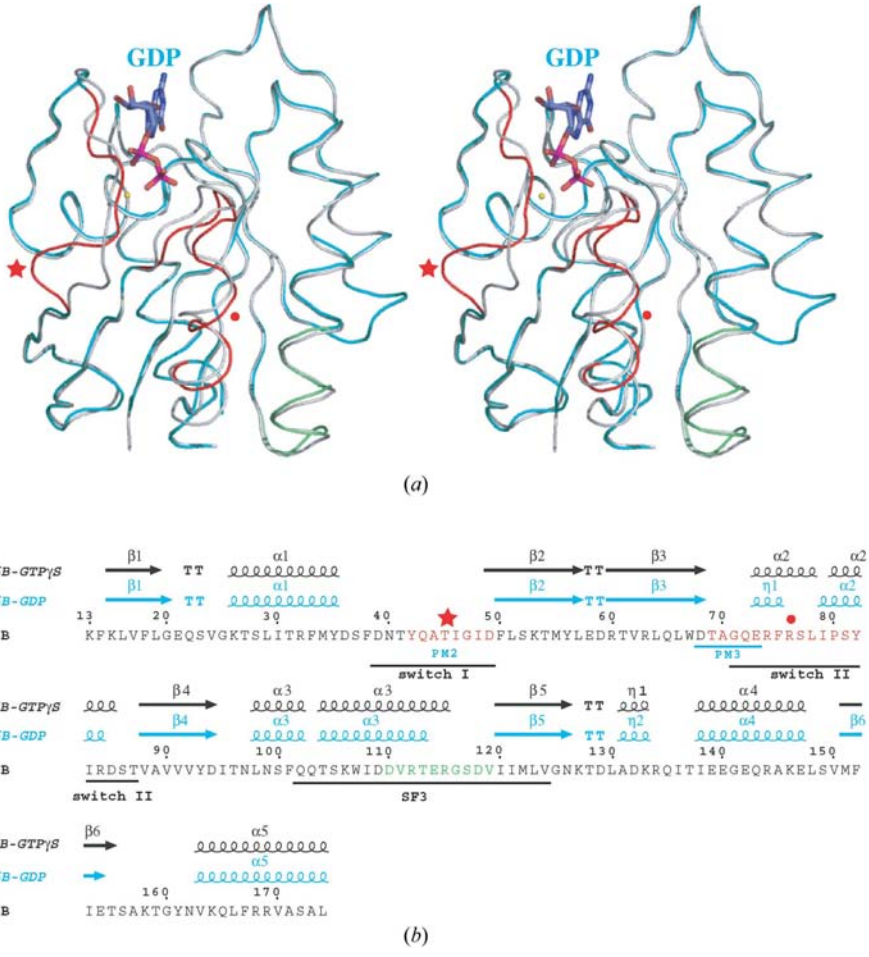

Figure 3
(*a*) Assignment of secondary-structural elements of Rab6B–GTPγS (grey) and Rab6B–GDP (blue). The areas of high flexibility (higher *B* factor) found in the Rab6B–GDP structure are highlighted in red (a star indicates the area of disorder around switch I and a circle indicates the area of disorder around switch II) and green (inside SF3 region). (*b*) Structural alignment of Rab6B–GTPγS and Rab6B–GDP following the same colour code.

4. Discussion

4.1. Differences between Rab6B–GDP and Rab6B–GTPγS

The GTPγS- and GDP-bound forms of Rab6B both crystallized in the same space group with similar unit-cell parameters and crystal packing, implying that the local differences found between both structures are intrinsically related to the nucleotide state of the protein. One modified region is located in the RabSF3 area. This includes the C-terminal part of helix α3 and the following loop which links to β5. The β-strand β5 is located in the core of the protein (no crystal contacts) and the α3 residues make only a few crystal contacts with symmetry-related molecules. We consider that the differences observed between the two structures, particularly in the RabSF3 region, cannot be explained by the effect of crystal packing since the intermolecular contacts are not extensive and part of the RabSF3 area (particularly the loop connecting to β5) faces the solvent with sufficient space in the lattice to permit free movement.

The main differences between the GDP and GTPγS forms arise from the absence of the γ-phosphate in the active

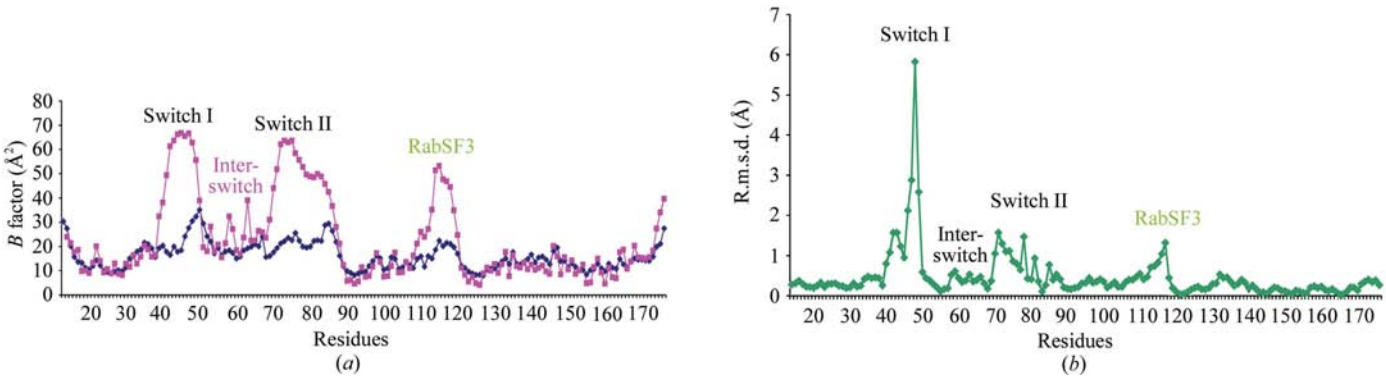

Figure 4
(*a*) Comparison of overall *B* factor per residue for the GTPγS-bound and GDP-bound forms of Rab6B. Average *B*-factor plots of Rab6B–GTPγS and Rab6B–GDP are depicted with diamonds and squares, respectively. The regions with high *B* factor in Rab6B–GDP (flexible, highly disordered regions) correspond to areas around switch I, interswitch, switch II and inside the subfamily-specific RabSF3 region (the C-terminal part of helix α3 followed by the connecting loop to β5). (*b*) Main-chain r.m.s.d. between GTPγS-bound and GDP-bound forms of Rab6B. The higher r.m.s.d. differences between both structures coincide with the regions of high temperature factors in Rab6B–GDP.

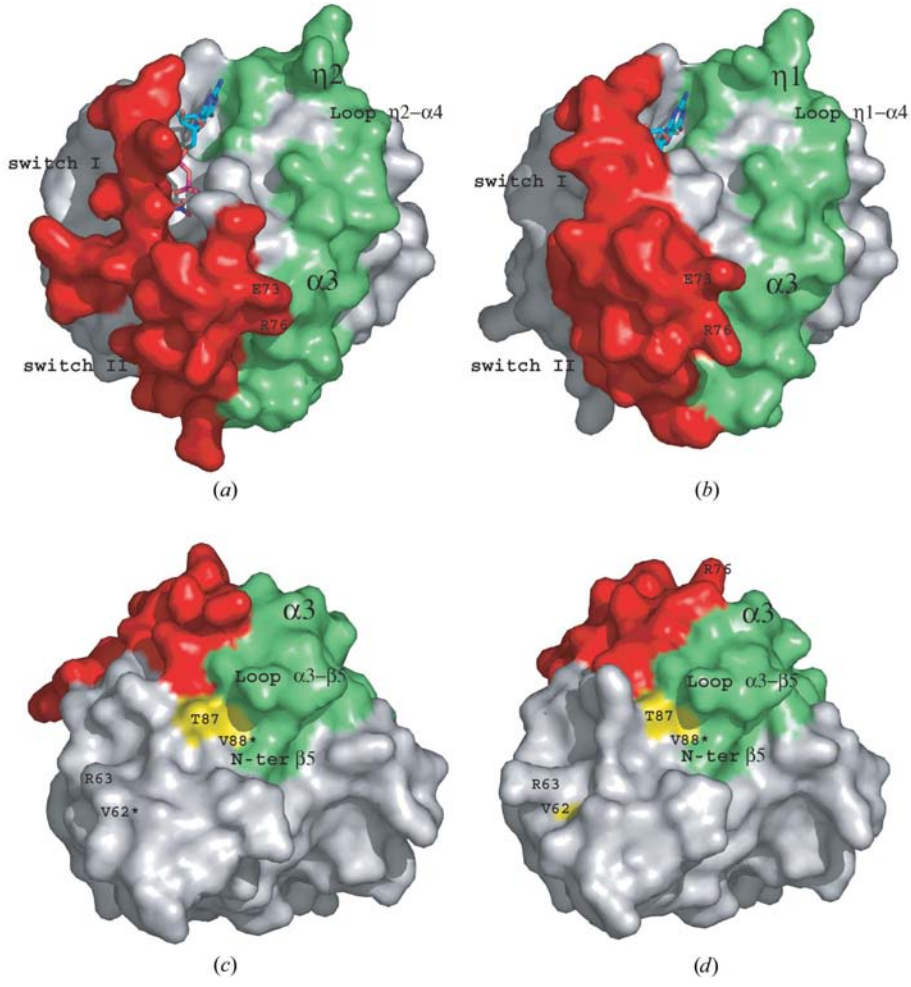

Figure 5
Surface representation of Rab6B–GDP (*a*, *c*) and Rab6B–GTPγS (*b*, *d*). The surface corresponding to the switch I and switch II regions is coloured in red. The neighbouring modified areas are depicted in green and include helix α3, the N-terminal area of β5, which forms the SF3 consensus domain, η1 (η2 in Rab6B–GDP) and guanine nucleotide-binding G2. (*c*) and (*d*) are views of (*a*) and (*b*) from below, respectively. The locations of the three residues that differ with respect to Rab6A′ are highlighted in yellow; an asterisk indicates that the residue is buried.

site. In the GTPγS-bound form (the 'well ordered' structure), the γ-phosphate makes contacts with residues from PM1 (Ser23 and Lys26), PM2 (Thr45), PM3 (Gly71, included in switch II), switch I (Tyr42), the Mg^{2+} ion and several water molecules.

One of the differences observed between the forms is in the binding to the main chain of Gly71 (switch II). The presence of γ-phosphate stabilizes the N-terminal part of helix α2 (switch II), since the tight binding of a γ-phosphate oxygen to the main-chain N of Gly71 (2.5 Å), which is located at the N-terminal tip of that helix, allows electrostatic interactions between the side chains of residues Arg74 and Gln72 and further stabilization of the helix. These interactions are absent in the GDP-bound structure (the closest distance between one of the nitrate O atoms and the main-chain N of Gly71 is 3.51 Å), giving rise to a very flexible region (destabilization of that part of α2 and formation of η1, illustrated in Fig. 3). Another difference is located at Tyr42 from switch I. The hydroxyl group of this Tyr interacts with the sulfur of GTPγS. This interaction is lost in the GDP-bound form, where Tyr42 moves away from the active site and rotates its side chain towards the solvent. This movement expands to the neighbouring residues of switch I, which shows very high disorder in the GDP-bound form. For example, in the GTPγS-bound form there are main-chain hydrogen bonds

between Asp49 (switch I) and Asp68 (PM3) that are absent in the GDP-bound form (where the only hydrogen bond is between the main chain of Ile48 and Phe50). But how do these differences affect the RabSF3 area? There is an interaction zone between switch II and RabSF3 in the structure. This area is localized at the C-terminal tips of helices $\alpha2$ and $\alpha3$, the connecting loop with $\beta5$ and the N-terminal part of $\beta5$. In the GTPγS form, because of the stabilization of helix $\alpha2$, there is a cluster of hydrogen bonds established between the side chains and main chains of Arg84, Ser86 and Thr87 (switch II) with Arg115, Glu114, Asp118 and Ile120 (RabSF3) which stabilize this area, at the same time promoting hydrogen bonds between Arg115 with Asp118 and Val119 with Ser170 (located in helix $\alpha5$). In the GDP-bound form these contacts are absent and the only conserved bond is that between the main-chain O atom of Arg84 and the side-chain NE of Arg115. Thus, in the GDP-bound form the destabilization of the N-terminus of $\alpha2$ expands and promotes the loss of bonds between residues of switch II and RabSF3, which generates a helix-to-coil transition at the C-terminal region of $\alpha2$ and $\alpha3$.

4.2. Comparison with other Rab proteins in the GDP- and GTP-bound forms

Several crystal structures of different Rab proteins in the active conformation with either GppNHp or GTPγS bound have been solved and these have been summarized in Eathiraj *et al.* (2005), but only a few in both the inactive GDP- and the active GTP-forms (Stroupe & Brunger, 2000; Constantinescu *et al.*, 2002; Zhu *et al.*, 2003; Pasqualato *et al.*, 2004; Huber & Scheidig, 2005), which would allow a more thorough analysis of the nucleotide-dependent conformational changes that determine specificity in effector recognition, have been determined. Structural superposition between our GDP-bound structure and various Rab proteins in the GDP-bound form has been performed (data not shown). The structures used were human Rab2A, Rab14, Rab21, Rab11A, mouse Rab23 (in two crystal forms) and Rab5C. In general, the main differences between Rab6B and these structures are located around the switches I and II and SF3 region and more particularly the C-terminal tip of helix $\alpha3$. Deviations are also located in the region between $\beta2$ and $\beta3$. Curiously, Val62, which is one of the three residues that differ in Rab6B compared with Rab6A′, is located in this turn. This residue is also Val in human Rab21, mouse Rab5C and Rab23, but Ile in human Rab11A, Rab2A and Rab14. The analysis is complicated by the fact that depending on the Rab protein, there is an enormous variability in the (Rab–GDP) switch regions as reviewed in Pfeffer (2005): Rab4a (only the GTP-bound form), Rab5 and Ypt7 have Mg^{2+} in the active site, whereas the magnesium ion is absent in Rab11 and is substituted by cobalt in Rab Sec4p. Rab11 is monomeric in the GTPγS-bound form, but becomes dimeric in the GDP-bound state, where the switch regions are stabilized by a large symmetric dimer interface. In addition, the GDP-bound forms of Rab Sec4p and Rab5 have been crystallized in two different forms with significant differences. Except for Rab5, for which the GTP- and GDP-bound forms crystallize in the same crystal form, all other nucleotide forms crystallize differently, thus making a direct comparison even more difficult since the observed conformational changes might be a consequence of different packing and contacts in the crystal. In our case, the Rab6B structures with GTPγS and GDP bound demonstrate clear differences, localized particularly in the switch region. The inactive GDP-bound form shows high disorder in this region, while the GTPγS-bound form, which simulates an active GTP-bound state, is well defined. From this observation, it can be hypothesized that the conformations of particular areas of Rab that occur in the GTP-bound form are necessary for effector recognition of binding motifs that otherwise would be inaccessible to the effector partner. By structural comparisons of both Rab6B states, confirmed by overall *B* factor per residue comparisons, we identified in the GDP-bound form a highly disordered area which interestingly coincides with RabSF3 (residues 109–121). A surface comparison between both forms also confirmed this observation (Fig. 5). Similarly, structural modelling performed on *P. falciparum* Rab6A′ showed that the exposed residue Ala87 (equivalent to Thr87 in Rab6B), the loop region of RabSF3 and the C-terminal part of RabF4 may provide a binding surface for the Rab6 effector (Quevillon *et al.*, 2003).

4.3. Comparison with structures of other members of the Rab6 subfamily

All Rab proteins solved to date have a very similar overall fold, but differ in subtle details that lead to specific recognition by their effector proteins. Structural superpositions using the entire Rab6B in the GTPγS-bound and GDP-bound forms with the available structures of other members of the Rab6 subfamily, *P. falciparum* Rab6A′–GDP (Chattopadhyay *et al.*, 2000) and *H. sapiens* Rab6A′–GppNHp (Eathiraj *et al.*, 2005), were performed.

The Rab6B sequence identity with *H. sapiens* Rab6A′ and *P. falciparum* Rab6A′ is 89 and 57%. The r.m.s.d. (for main-chain atoms) between Rab6B–GTPγS, *Plasmodium* Rab6A′–GDP and human Rab6A′–GppNHp are 1.2 and 1.0 Å, respectively. For Rab6B–GDP, these values are 1.1 and 1.2 Å.

The structural comparison between Rab6B–GDP and *P. falciparum* Rab6A′–GDP showed that the main differences are located around the switch I (r.m.s.d. 3.9 Å), interswitch (r.m.s.d. 1.9 Å) and to a lesser extent the switch II (r.m.s.d. 1.4 Å) and RabSF3 (1.5 Å) areas.

Comparison of Rab6B–GTPγS with human Rab6A′–GppNHp showed that the region with highest deviation (r.m.s.d. of 2.6 Å) was the interswitch region (between Thr54 and Arg63). It is precisely in this area where there is a one-residue difference (Val62 in Rab6B and Ile62 in Rab6A′) that affects the short loop connecting strands $\beta2$ and $\beta3$ and that may be one of the residues involved in Rabkinesin-6 effector recognition. In Rab6B this turn is shorter since the presence of Val62 in this predominantly hydrophobic area stabilizes the β-sheet interactions between $\beta2$ and $\beta3$ strands. The presence of the slightly bulkier Ile in Rab6A′ promotes the formation of a

longer turn which runs almost perpendicular with respect to the turn in Rab6B. There are also two other residues that differ between human Rab6B and Rab6A′. They are located immediately after the switch II consensus sequence (Thr87 and Val88 in Rab6B and Ala87 and Ala88 in Rab6A′; Figs. 5*c* and 5*d*). Other residues which differ in both isoforms are outside the switch regions and do not promote any major structural changes, although it cannot be ruled out that they may be involved in effector recognition. Surprisingly, and despite a very high sequence similarity, the surface areas defined in both Rab6B and Rab6A′ structures present subtle differences that could explain the different effector selectivity for Rabkinesin-6. Rab6–effector interaction may be based mainly on surface–surface complementarity recognition, stabilized by further polar and hydrophobic interactions.

We thank Jean-Pierre Andrieu (Laboratoire d'Enzymologie Moléculaire, LIM) for N-terminal protein sequencing of Rab6B and Dr David Lemaire as well as Sebastien Brier (both at the Laboratoire de Spectrométrie de Masse des Protéines, LSMP) for mass-spectrometric analysis. We are grateful to José Márquez (EMBL-Grenoble) and his crystallization service for using the nanodrop robot to find initial crystallization conditions. We also want to thank the staff at ID-14 and BM30A (ESRF-Grenoble) for technical assistance at the beamlines. This work has been funded by grants from SPINE (Structural Proteomics In Europe, contract No. QLG2-CT-2002-00988 to FK) and ARC (Association pour la Recherche sur le Cancer to ST).

References

Bock, J. B., Matern, H. T., Peden, A. A. & Scheller, R. H. (2001). *Nature (London)*, **409**, 839–841.

Brünger, A. T., Adams, P. D., Clore, G. M., DeLano, W. L., Gros, P., Grosse-Kunstleve, R. W., Jiang, J.-S., Kuszewski, J., Nilges, M., Pannu, N. S., Read, R. J., Rice, L. M., Simonson, T. & Warren, G. L. (1998). *Acta Cryst.* D**54**, 905–921.

Chattopadhyay, D., Langsley, G., Carson, M., Recacha, R., DeLucas, L. & Smith, C. (2000). *Acta Cryst.* D**56**, 937–944.

Collaborative Computational Project, Number 4 (1994). *Acta Cryst.* D**50**, 760–763.

Constantinescu, A. T., Rak, A., Alexandrov, K., Esters, H., Goody, R. S. & Scheidig, A. J. (2002). *Structure*, **10**, 569–579.

Cuif, M. H., Possmayer, F., Zander, H., Bordes, N., Jollivet, F., Couedel-Courteille, A., Janoueix-Lerosey, I., Langsley, G., Bornes, M. & Goud, B. (1999). *EMBO J.* **18**, 1772–1782.

DeLano, W. L. (2002). *The PyMOL Molecular Graphics System.* DeLano Scientific, San Carlos, CA, USA.

Eathiraj, S., Pan, X., Ritacco, C. & Lambright, D. G. (2005). *Nature (London)*, **436**, 415–419.

Echard, A., Jollivet, F., Martinez, O., Lacapere, J. J., Rousselet, A., Janoueix-Lerosey, I. & Goud, B. (1998). *Science*, **279**, 580–585.

Echard, A., Opdam, F. J., de Leeuw, H. J., Jollivet, F., Savelkoul, P., Hendriks, W., Voorberg, J., Goud, B. & Fransen, J. A. (2000). *Mol. Biol. Cell*, **11**, 3819–3833.

Fontijn, R. D., Goud, B., Echard, A., Jollivet, F., van Marle, J., Pannekoek, H. & Horrevoets, A. J. (2001). *Mol. Cell. Biol.* **21**, 2944–2955.

Gouet, P., Courcell, E., Stuart, D. I. & Metoz, F. (1999). *Bioinformatics*, **15**, 305–308.

Hirel, P. H., Schmitter, M. J., Dessen, P., Fayat, G. & Blanquet, S. (1989). *Proc. Natl Acad. Sci. USA*, **85**, 8247–8251.

Huber, S. K. & Scheidig, A. J. (2005). *FEBS Lett.* **579**, 2821–2829.

Lai, F., Fernald, A. A., Zhao, N. & Le Beau, M. M. (2000). *Gene*, **248**, 117–125.

Laskowski, R., MacArthur, M., Moss, D. & Thornton, J. (1993). *J. Appl. Cryst.* **26**, 283–291.

Mallard, F., Tang, B. L., Galli, T., Tenza, D., Saint-Pol, A., Yue, X., Antony, C., Hong, W., Goud, B. & Johannes, L. (2002). *J. Cell Biol.* **156**, 653–664.

Martinez, O., Schmidt, A., Salamero, J., Hoflack, B., Roa, M. & Goud, B. (1994). *J. Cell Biol.* **127**, 1575–1588.

Monier, S., Jollivet, F., Janoueix-Lerosey, I., Johannes, L. & Goud, B. (2002). *Traffic*, **3**, 289–297.

Moore, I., Schell, J. & Palme, K. (1995). *Trends Biochem. Sci.* **20**, 10–12.

Navaza, J. & Saludjian, P. (1997). *Methods Enzymol.* **276**, 581–594.

Opdam, F. J., Echard, A., Croes, H. J., van den Hurk, J. A., van de Vorstenbosch, R. A., Ginsel, L. A., Goud, B. & Fransen, J. A. (2000). *J. Cell Sci.* **113**, 2725–2735.

Otwinowski, Z. & Minor, W. (1997). *Methods Enzymol.* **276**, 307–326.

Pasqualato, S., Senic Matuglia, F., Renault, L., Goud, B., Salamero, J. & Cherfils, J. (2004). *J. Biol. Chem.* **279**, 11480–11488.

Pereira-Leal, J. B. & Seabra, M. C. (2000). *J. Mol. Biol.* **301**, 1077–1087.

Pfeffer, S. R. (2005). *J. Biol. Chem.* **280**, 15485–15488.

Quevillon, E, Spielmann, T., Brahimi, K., Chattopadhay, D., Yeramian, E. & Langsley, G. (2003). *Gene*, **306**, 13–25.

Roussel, A. & Cambillau, C. (1991). *Silicon Graphics Geometry Partners Directory*, p. 86. Mountain View, CA, USA: Silicon Graphics.

Shan, J., Mason, J. M., Yuan, L., Barcia, M., Porti, D., Calabro, A., Budman, D., Vinciguerra, V. & Xu, H. (2000). *Gene*, **257**, 67–75.

Stroupe, C. & Brunger, A. T. (2000). *J. Mol. Biol.* **304**, 585–598.

Takai, Y., Sasaki, T. & Matozali, T. (2001). *Physiol. Rev.* **81**, 153–208.

Teber, I., Nagano, F., Kremerskothen, J., Bilbilis, K., Goud, B. & Barnekow, A. (2005). *Biol. Chem.* **386**, 671–677.

White, J., Johannes, L., Mallard, F., Girod, A., Grill, S., Reinsch, S., Keller, P., Tzschaschel, B., Echard, A., Goud, B. & Stelzer, E. H. (1999). *J. Cell Biol.* **147**, 743–760.

Zahraoui, A., Touchot, N., Chardin, P. & Tavitian, A. (1989). *J. Biol. Chem.* **264**, 12394–12401.

Zerial, M. & McBride, H. (2001). *Nature Rev. Mol. Cell Biol.* **2**, 107–117.

Zhu, G., Liu, J., Terzyan, S., Zhi, P., Li, G. & Zhang, X. C. (2003). *J. Biol. Chem.* **278**, 2452–2460.